

An Image is Worth Multiple Words: Multi-attribute Inversion for Constrained Text-to-Image Synthesis

Aishwarya Agarwal, Srikrishna Karanam, Tripti Shukla, and Balaji Vasan Srinivasan
Adobe Research, Bengaluru India

{aishagar, skaranam, trshukla, balsrini}@adobe.com

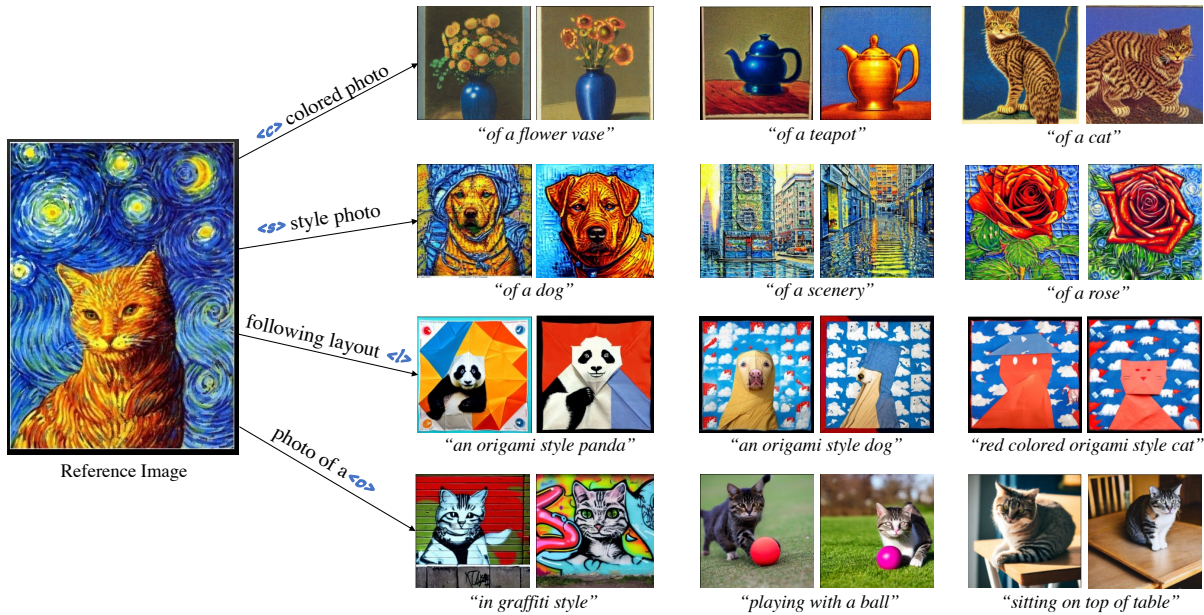


Figure 1: Given a single reference image, we propose a new algorithm MATTE to extract four tokens, one each for color, style, object, and layout properties of the image. They can then be used for attribute-guided image synthesis as shown in columns 2-4.

Abstract

We consider the problem of constraining diffusion model outputs with a user-supplied reference image. Our key objective is to extract multiple attributes (e.g., color, object, layout, style) from this single reference image, and then generate new samples and novel compositions with them. One line of existing work proposes to invert these reference images into a single textual conditioning vector, enabling generation of new samples with this learned token. These methods, however, do not learn multiple tokens that are necessarily required to condition model outputs on the multiple attributes noted above. Another line of techniques expand the inversion space to learn multiple embeddings but they do this only along the layer dimension (e.g., one per layer of the DDPM model) or the timestep dimension (one for a set of timesteps in the denoising process), leading to suboptimal attribute disentanglement.

To address the aforementioned gaps, the first contribution of this paper is an extensive analysis to determine which attributes are captured in which dimension of the denoising process. As noted above, we consider both the time-step di-

mension (in reverse denoising) as well as the DDPM model layer dimension. We observe that often a subset of these attributes are captured in the same set of model layers and/or across same denoising timesteps. For instance, color and style are captured across same U-Net layers, whereas layout and color are captured across same timestep stages. Consequently, an inversion process that is designed only for the time-step dimension or the layer dimension is insufficient to disentangle all attributes. This leads to our second contribution where we design a new multi-attribute inversion algorithm, **MATTE**, with associated disentanglement-enhancing regularization losses, that operates across both dimensions and explicitly leads to four disentangled tokens (color, style, layout, and object). We conduct extensive evaluations to demonstrate the effectiveness of the proposed approach.

1 Introduction

We consider the text-to-image class of generative diffusion models (Ho, Jain, and Abbeel 2020; Rombach et al. 2022; Sohl-Dickstein et al. 2015; Song, Meng, and Ermon 2020)

and explore the problem of conditioning them based on a user-supplied reference image. In particular, we seek to extract multiple attributes (*color*, *object*, *style*, and *layout*) from the reference to synthesize images with any combination of these learned attributes. While there has been much work in personalizing text-to-image diffusion models (Gal et al. 2022; Ruiz et al. 2023; Kumari et al. 2023; Voynov et al. 2023; Zhang et al. 2023), they lack explicit control on which attributes from the reference are to be reflected in the model outputs. For instance, one line of recent work (Gal et al. 2022; Ruiz et al. 2023; Kumari et al. 2023) inverted the reference image into a single learned token and used it to synthesize new samples. Since this process learned only a single conditioning vector, it was not able to disentangle the inherently multi-attribute information from the reference image (e.g., *color*, *object*, *layout*, and *style* all constitute complementary and separate pieces of information). Consequently, these techniques only generate more samples “like” the reference but fail if we seek more control (e.g., in synthesizing samples that follow the *color*, or *style*, or *layout* and *object* of the reference, etc.).

There have also been attempts to expand the inversion space by learning multiple token embeddings. For instance, P+ (Voynov et al. 2023) learned these tokens by inverting the reference image along all the 16 cross-attention layers of the DDPM model (Ronneberger, Fischer, and Brox 2015), whereas ProSpect (Zhang et al. 2023) inverted the reference image along the denoising timestep dimension by dividing the steps into 10 stages. As we discuss next, even these strategies are insufficient to disentangle all attributes.

First, the key findings from P+ (Voynov et al. 2023) were that semantic information is captured in coarse layers of the DDPM model (U-Net (Ronneberger, Fischer, and Brox 2015)) whereas appearance information (e.g., *color*) is captured in the shallow layers. However, as we will show in our work, *layout* and *object* semantics are captured in the same set of coarse layers of the DDPM model whereas *color* and *style* share the same set of shallow layers. This suggests that the attempted disentanglement in P+ (Voynov et al. 2023) by learning multiple tokens across the DDPM layer dimension is insufficient because such an inversion space will not disentangle *color* from *style* and *layout* from *object*. To understand this clearly, consider the example shown in Figure 2. Here, we invert the elephant reference image using the P+ (Voynov et al. 2023) technique and synthesize new images by modifying either of the coarse or shallow layers. The synthesized images in the first row show that they have *both* *object* and *layout* semantics from the reference image and cannot be conditioned on either of them individually since they are captured in the same set of DDPM model layers. Similar observations hold for the *color* and *style* pair as well since they are captured in the same set of layers (see second row in Figure 2).

Next, ProSpect (Zhang et al. 2023) proposed to divide the denoising process into several stages (each comprising a few timesteps) and concluded that attributes like *color* and *layout* are captured in the beginning (first several timesteps), *object* semantics towards the middle, and fine-grained details towards the end of the denoising process.

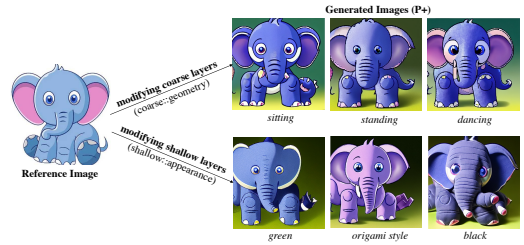


Figure 2: Attribute entanglement in P+ (Voynov et al. 2023).

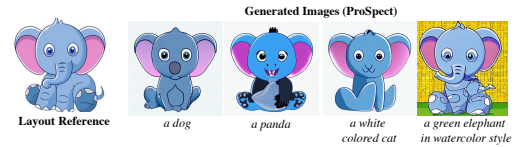


Figure 3: Attribute entanglement in ProSpect.

As we will show in our work, the *style* attribute is also captured in the first few timesteps, thereby making it challenging to disentangle *color*, *layout*, and *style* if we consider only this timestep dimension when learning these tokens. To understand this clearly, consider the example in Figure 3, where we use the reference image (first column) of a *pinkish blue cartoon style elephant* for text-to-image generation. In the synthesized images (columns 2-5), one can note they follow not only the *layout* but also the *color* and *style* information from the reference image, suggesting no disentanglement among these attributes has happened after learning tokens with ProSpect (Zhang et al. 2023).

U-Net layers		Denoising timesteps				
		0-200 (t_1)	200-400 (t_2)	400-800 (t_3)	800-1000 (t_4)	
fine	L ₁	64	null	null	null	null
	L ₂	64				
moderate	L ₃	32	red, cat, sitting	null	null	null
	L ₄	32				
coarse	L ₅	16	green, cat, standing	cat	cat	cat
	L ₆	16				
moderate	L ₇	8	red, cat, sitting	null	null	null
	L ₈	16				
	L ₉	16				
	L ₁₀	16				
fine	L ₁₁	32	null	null	null	null
	L ₁₂	32				
	L ₁₃	32				
	L ₁₄	64				
fine	L ₁₅	64	null	null	null	null
	L ₁₆	64				
	L ₁₇	64				



Figure 4: Layout-Color disentanglement.

Based on the aforementioned observations and limitations of P+ (Voynov et al. 2023) and ProSpect (Zhang et al. 2023), the key insight of this paper is that an inversion strategy solely focused on either the layer dimension or the denoising timestep dimension is insufficient to disentangle all our attributes of interest from a reference image and use them for controlled text-to-image synthesis. In fact, we need to consider both dimensions *jointly* when designing an inversion strategy so as to learn meaningful individual attribute tokens for subsequent synthesis. To this end, the key contributions of this paper are two-fold. First, we conduct an

extensive and exhaustive layer-and-timestep analysis to determine which layers and which timesteps influence what attributes during the generation process. While we discuss complete details in Section 3.1, we present some sample results here. In Figure 10, we show all the 16 cross-attention layers of the DDPM U-Net model (Ronneberger, Fischer, and Brox 2015) as well as four different stages ($t_1 - t_4$) of the denoising process. Here, based on the final generated image (a red standing cat), one can note that the text conditions corresponding to the color `red` were specified in the $L_3 - L_5$ & $L_{10} - L_{13}$ layers (see first column, t_1 stage) and had the most impact on the final image. For instance, despite the input `green` in $L_6 - L_9$ layers, the final image has a red cat. Similarly, despite specifying the layout `sitting` in layers $L_3 - L_5$ & $L_{10} - L_{13}$, the final generation only respected `standing` that was provided to $L_6 - L_9$. This shows that while `color` and `layout` are captured along the same timesteps (from Prospect (Zhang et al. 2023)), they can be disentangled along the layer dimension ($L_3 - L_5$ & $L_{10} - L_{13}$ for color and $L_6 - L_9$ for layout).

Informed by results like those above, our second contribution is a new **Multi-Attribute Inversion** algorithm called **MATTE** that is explicitly designed to consider both the DDPM model layer and the denoising timestep dimension as part of the learning process. Specifically, we propose four new learnable tokens, one for each of `color`, `object`, `layout`, and `style`, and design our learning objectives so that each of the four tokens are trained to influence either separate layers in the model or separate timesteps in the denoising process. Figure 1 shows our results with the individual $\langle c \rangle$, $\langle o \rangle$, $\langle s \rangle$, and $\langle l \rangle$ tokens. Using them as part of new prompts leads to meaningful results (e.g., flower vase/teapot/cat in first row follow the color $\langle c \rangle$ of the reference, the dog/scenery/rose in second row follow the style $\langle s \rangle$ of the reference, we get cat images with object $\langle o \rangle$ as desired in the last row and so on).

To summarize, the key contributions of this paper are:

- We present an extensive multi-attribute disentanglement analysis jointly across both the DDPM model layer dimension and the reverse denoising timestep dimension to understand which attributes are captured at which stage and along which dimension during the generation process, thereby discovering reasons why existing inversion algorithms fail as shown in Figures 2 and 3.
- We present a novel multi-attribute inversion algorithm with four learnable tokens (for color, object, layout, and style attributes) and a principled approach to disentangling them, allowing for attribute-guided synthesis based on reference images.

2 Related Work

Since the emergence of large-scale diffusion models for conditional image synthesis (Nichol et al. 2021; Rombach et al. 2022; Ramesh et al. 2022; Saharia et al. 2022), there has been much recent work in adapting these models with a variety of conditioning types (Zhang and Agrawala 2023; Mou et al. 2023). One particular line of work has been personalized inversion where a reference image is used to learn

conditioning vectors to be used with novel prompts. Gal et al. (Gal et al. 2022) proposed a first baseline version that learned a single vector for a new token (while keeping diffusion model weights fixed), which could then be used to synthesize novel personalized variations of the reference image. On the other hand, methods like Dreambooth (Ruiz et al. 2023), CustomDiffusion (Kumari et al. 2023), and Perfusion (Tewel et al. 2023) involved finetuning the weights of the diffusion model. Inversion has been explored in GANs too (Bermano et al. 2022; Creswell and Bharath 2018; Lipton and Tripathi 2017; Xia et al. 2022) with both latent optimization (Abdal, Qin, and Wonka 2019, 2020) and model finetuning methods (Alaluf et al. 2022; Roich et al. 2022; Nitzan et al. 2022).

Our closest baselines include P+ (Voynov et al. 2023) and Prospect (Zhang et al. 2023), both of which enhanced the inversion space by learning more than one conditioning vector. However, they are unable to disentangle all our attributes of interest. In P+ (Voynov et al. 2023), while tokens are learned by inverting the reference image along all the 16 cross-attention layers of the DDPM model, disentanglement of color from style and layout from object is impossible because the layout/object pair and the color/style pair are captured in the same set of layers of the DDPM model. On the other hand, in Prospect (Zhang et al. 2023), while tokens are learned by dividing the denoising process into multiple timestep stages, it is not able to disentangle color, layout, and object since they are all captured in the same timestep stages. To address these issues, our proposed inversion algorithm introduces new per-attribute tokens and optimizes them jointly across both layer and timestep dimension, enabling multi-attribute extraction from a reference image and synthesizing novel compositions using them.

3 Approach

3.1 Layer-timestep Attribute Disentanglement

Our first contribution is an extensive analysis of text-to-image diffusion models to understand which layers (in the DDPM model) and timesteps (in backward process) jointly are responsible for capturing attributes (we consider `color`, `style`, `layout`, `object`) during generation. As discussed in Section 1 previously, either P+ (Voynov et al. 2023) or Prospect (Zhang et al. 2023) are unable to disentangle all attributes. To understand why and how that leads to our method in Section 3.2, we analyze the attribute distribution during the generation process jointly across both the layer and timestep dimensions. To this end, let us consider the example shown in Figure 5. The U-Net (Ronneberger, Fischer, and Brox 2015) that is used in the DDPM model of Stable Diffusion (Rombach et al. 2022) comprises 16 cross-attention layers of resolutions 8, 16, 32, and 64 (see the figure for per-layer resolution). We partition them into three sets: coarse ($L_6 - L_9$), moderate ($L_3 - L_5$ & $L_{10} - L_{13}$), and fine ($L_1 - L_2$ & $L_{14} - L_{16}$). Similarly, we partition the denoising timesteps into four stages: t_1 , t_2 , t_3 and t_4 . We seek to understand the timesteps and layers where the four attributes are captured during the generation process. To do this, we propose to add/remove conditioning from both timesteps and layers and analyze the output.

U-Net layers		Denoising timesteps			
		0-200 (t_1)	200-400 (t_2)	400-800 (t_3)	800-1000 (t_4)
fine	L_1	blue, lizard, sitting, graffiti style	blue, lizard, sitting, graffiti style	blue, lizard, sitting, graffiti style	blue, lizard, sitting, graffiti style
	L_2				
moderate	L_3	<i>red</i> , lizard, sitting, <i>oil painting style</i>	<i>red</i> , lizard, sitting, <i>oil painting style</i>	white, lizard, sitting, graffiti style	white, lizard, sitting, graffiti style
	L_4				
	L_5				
course	L_6	green, cow, <i>standing</i>	green, <i>cat</i> , sitting	green, <i>cat</i> , sitting	green, cow, sitting
	L_7				
moderate	L_8	<i>red</i> , lizard, sitting, <i>oil painting style</i>	<i>red</i> , lizard, sitting, <i>oil painting style</i>	white, lizard, sitting, graffiti style	white, lizard, sitting, graffiti style
	L_9				
	L_{10}				
	L_{11}				
fine	L_{12}	blue, lizard, sitting, graffiti style	blue, lizard, sitting, graffiti style	blue, lizard, sitting, graffiti style	blue, lizard, sitting, graffiti style
	L_{13}				
	L_{14}				
	L_{15}				
	L_{16}				



Figure 5: Multi-prompt conditioning across U-Net layers and denoising timesteps jointly.

In Figure 5, we show results for one case of joint prompting across both layers and the denoising stages. For the final generated image (*a red standing cat in oil painting style*), one can note that the textual conditionings corresponding to each of key attributes in the prompt (*red*, *standing*, *cat*, and *oil painting*) were specified only across a subset of layers and only along specific timesteps. In fact, despite specifying *blue* in $L_1 - L_2$ & $L_{14} - L_{16}$ layers, we still see a *red* colored cat, suggesting the existence of some patterns in how these attributes are distributed across layers and time stages. We next discuss them:

- **Color:** Specifying colors like *green* and *blue* in conditioning for fine ($L_1 - L_2$ & $L_{14} - L_{16}$) and coarse layers ($L_6 - L_9$) respectively has no impact on the generated image (which is *red*). Similarly, colors like *white* in the later denoising stages (t_3, t_4) of moderate layers ($L_3 - L_5$ & $L_{10} - L_{13}$) has no impact on the final generation and we indeed get a *red* cat. This indicates that *color* is captured in the initial denoising stages (t_1, t_2) across the moderate layers ($L_3 - L_5$ & $L_{10} - L_{13}$).
- **Style:** This is similar to color. Specifying *graffiti* and *watercolor* styles across coarse ($L_6 - L_9$) and fine ($L_1 - L_2$ & $L_{14} - L_{16}$) layers, and *graffiti* towards the later denoising stages (t_3, t_4) has no impact on the generated image. The image is still based on *oil painting* from (t_1, t_2) across ($L_3 - L_5$ & $L_{10} - L_{13}$).
- **Object:** A *cat* is generated despite specifying *cow* in the initial and later stages (t_1, t_4), suggesting *object* is captured in the middle stages (t_2, t_3). Coarse layers ($L_6 - L_9$) seem to be responsible because specifying other types like *lizard* in other layers have no impact.
- **Layout:** We can see that changing the layout aspects from *standing* to *sitting* after the first denoising stage has no impact on the posture of the cat being generated. This indicates *layout* is captured in the initial stages (t_1). Moreover, only the layers with resolution 16 are responsible. In particular, based on the per-layer cross-attention maps across timesteps in Figure 6, one

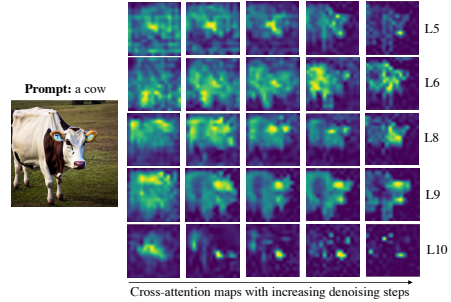


Figure 6: Cross-attention maps for analyzing layout.

can note layout properties are predominantly captured across the initial few timesteps in layers L_6, L_8 , and L_9 .

To summarize, fine layers ($L_1 - L_2$ & $L_{14} - L_{16}$) and the stage t_4 have no impact on any of the four attributes. *Color* and *style* are both captured in the initial denoising stages (t_1, t_2) and across moderate U-Net layers ($L_3 - L_5$ & $L_{10} - L_{13}$). *Object* semantics are captured along the middle denoising stages (t_2, t_3) and across the coarse U-Net layers ($L_6 - L_9$). Finally, *layout* is captured in the very initial denoising stage (t_1) across coarse layers ($L_6 - L_9$).

3.2 MATTE: Multi-Attribute Inversion

Given a reference image and a base text-to-image diffusion model, the second contribution of this paper is MATTE, a new inversion algorithm that extracts a set of four tokens $\langle c \rangle$, $\langle o \rangle$, $\langle s \rangle$, and $\langle l \rangle$ for the color, object, style, and layout attributes respectively. Our algorithm design is motivated by the conclusions in Section 3.1 and explicitly considers both the DDPM model layer and the timestep dimension jointly as part of the token learning process. This essentially means that the textual condition vectors in our algorithm vary across both U-Net layer dimension as well as the timestep dimension. Note that this is different from P+ (Voynov et al. 2023) where these vectors were dif-

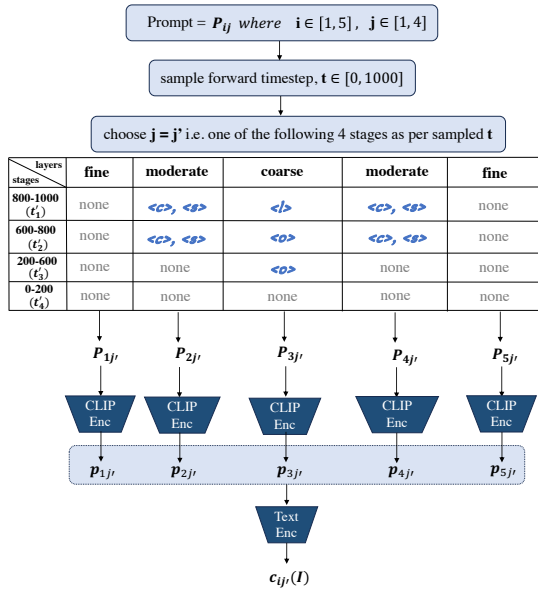


Figure 7: Computing the input conditioning in MATTE.

ferent only for the U-Net layers and Prospect (Zhang et al. 2023) where these vectors were different only for different timesteps of the reverse denoising process. As summarized in Section 3.1, our key insight is that we can disentangle all the four attributes only when we consider both layer and timestep dimension jointly as part of the learning process.

To this end, we divide the U-Net into *coarse*, *moderate* and *fine* layers and the forward diffusion process of 1000 steps into four stages t'_1 (800-1000), t'_2 (600-800), t'_3 (200-600), t'_4 (0-200). Note that t'_1, t'_2, t'_3, t'_4 in forward diffusion corresponds to the t_1, t_2, t_3, t_4 (notation used in Section 3.1) respectively of the backward denoising process. Hence, properties of backward denoising stages translate directly to the corresponding forward diffusion stages. We summarize the salient features of our algorithm in Figure 7. We use P_{ij} to specify how the input prompt translates to the conditioning vector. The $i \in [1, 5]$ corresponds to the five layer subsets (shown in Figure 7) whereas $j \in [1, 4]$ corresponds to the four timestep stages. Consequently, P_{ij} comprises of a set 4 different prompts, one for each timestep stage, where each of further comprises 5 prompts for conditioning each layer subset differently. Figure 7 also shows how our learnable tokens $\langle c \rangle$, $\langle o \rangle$, $\langle s \rangle$, and $\langle l \rangle$ are part of the input prompt across the various layers and timestep stages. For instance, as noted in Section 3.1, the *object* feature get captured only in the coarse layers ($L_6 - L_9$) and the middle t_2, t_3 backward denoising stages. Consequently, one can note the token $\langle o \rangle$ is explicitly designed to condition only the coarse layers and the forward t'_2, t'_3 diffusion stages. This means if the sampled timestep $t \in t'_3$ in the forward diffusion process, only then will $\langle o \rangle$ end up influencing the final conditioning vector across the coarse U-Net layers. Similar observations can be derived from Figure 7 for $\langle c \rangle$, $\langle s \rangle$, and $\langle l \rangle$ tokens. Subsequently, during inversion, for a particular backward pass, depending

on the sampled timestep, the embeddings corresponding to only active tokens from Figure 7 end up being optimized.

MATTE’s learning objective comprises three parts. The first part is the standard reconstruction loss:

$$\mathcal{L}_{\mathcal{R}} = \mathbb{E}_{z \sim E(I), t, p, \epsilon \sim \mathcal{N}(0,1)} [\|\epsilon - \epsilon_{\Theta}(z_t, t, p_j)\|_2^2], \quad (1)$$

where p_j comprises learnable embeddings for a subset of the $\langle c \rangle$, $\langle o \rangle$, $\langle s \rangle$, and $\langle l \rangle$ tokens depending on the sampled timestep $t \in [0, 1000]$ in the forward diffusion process. Next, *color* and *style* attributes are captured across the same layers and the timestep stages (see also Figure 7). Consequently, we propose an additional color-style disentanglement loss to help disentangle these tokens:

$$\mathcal{L}_{CS} = \|\mathbf{c} - \mathbf{s}\|_2^2 - \|\mathbf{c}_{gt} - \mathbf{s}\|_2^2, \quad (2)$$

where \mathbf{c} is the encoded vector of token $\langle c \rangle$, \mathbf{s} is the encoded vector for any randomly chosen style from a set of 30 styles like watercolor, graffiti, oil painting and so on (see supp. for full set of styles), and \mathbf{c}_{gt} is the CLIP (Radford et al. 2021) embedding of all the ground truth colors in the reference image (which we extract using the Color Thief (Dhakar 2015) library). Our intuition is to push the learned embedding \mathbf{c} for $\langle c \rangle$ close to \mathbf{c}_{gt} by ensuring both are equally distant from \mathbf{s} . This process naturally pushes $\langle c \rangle$ ’s embedding to be close to the CLIP feature space of colors (and hence different from the embedding for $\langle s \rangle$).

Finally, from Section 3.1 and Figure 7, *object* and *layout* inform the same set of coarse U-Net layers. To further disentangle $\langle o \rangle$ and $\langle l \rangle$, we propose a regularization on the learned token for $\langle o \rangle$ by ensuring it respects the class of the object depicted in the reference image. We do this by computing the ground-truth class label’s CLIP vector and enforcing it to be close to $\langle o \rangle$ ’s vector:

$$\mathcal{L}_O = \|\mathbf{o} - \mathbf{o}_{gt}\|_2^2 \quad (3)$$

where \mathbf{o} is the learned vector for token $\langle o \rangle$ and \mathbf{o}_{gt} is the ground truth. MATTE’s overall loss function is:

$$\mathcal{L}_{inv} = \mathcal{L}_{\mathcal{R}} + \lambda_{CS} \mathcal{L}_{CS} + \lambda_O \mathcal{L}_O \quad (4)$$

where $\lambda_{CS} = \lambda_O = 0.1$

4 Results

Qualitative Evaluation. In addition to the results in Figure 1, we show more results with MATTE in Figure 8 (reference image in first column and our results in columns two-five) to demonstrate multi-attribute transfer from a reference image (all embeddings for $\langle c \rangle$, $\langle l \rangle$, $\langle o \rangle$, $\langle s \rangle$ are learned with the proposed Equation 4). In the first row/second column, by specifying $\langle c \rangle$ and $\langle o \rangle$ in the input, we are able to generate new cat images in watercolor style following colors of the reference. Similarly, in the last column, we are able to generate new images of a bottle in watercolor style in $\langle c \rangle$ colors. In the second row/first column, MATTE is able to correctly infer the layout and the object from the reference in synthesizing new images of pebbles stacked on top of each other. Finally, in the third row/third column, MATTE infers the pencil sketch style ($\langle s \rangle$) of a

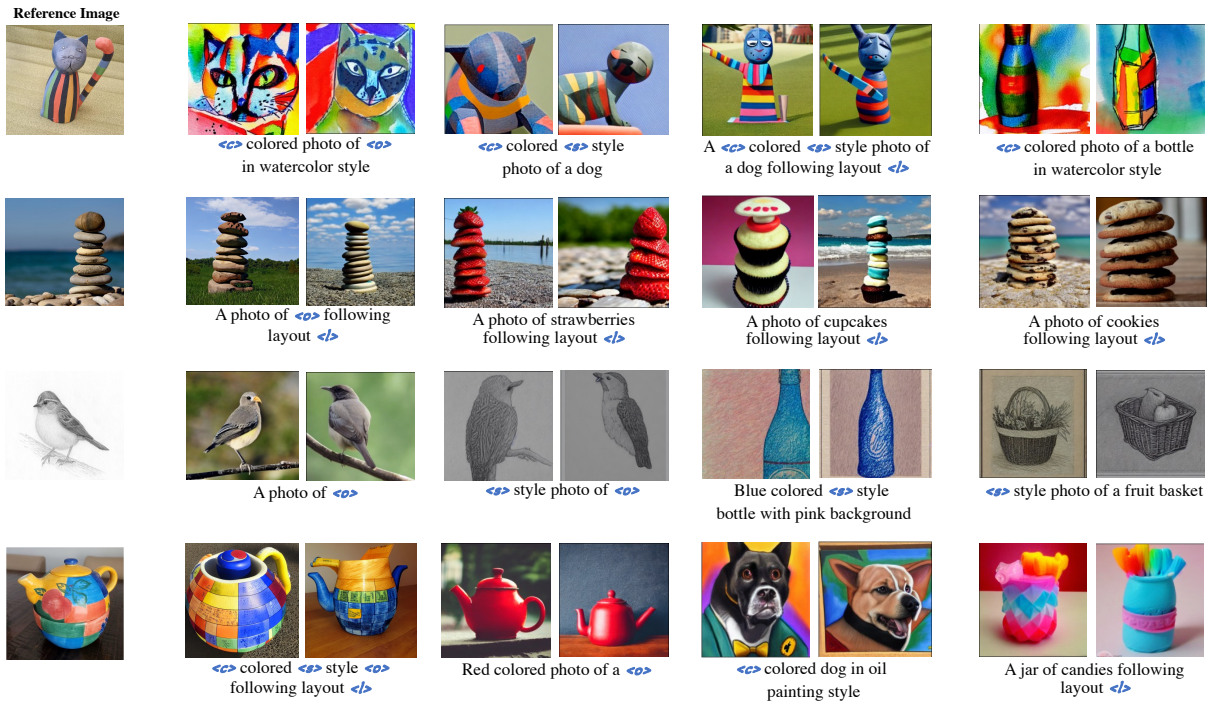


Figure 8: Qualitative results demonstrating multi-attribute transfer using MATTE from a reference image.

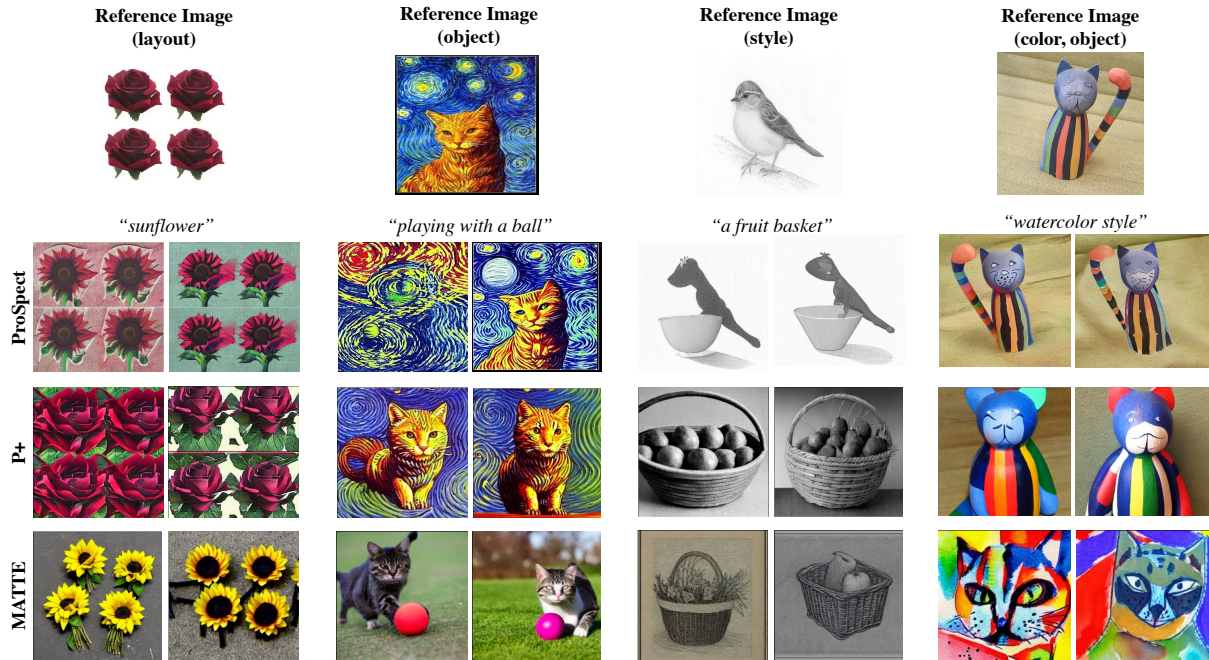


Figure 9: Comparison of MATTE with recent state-of-the-art methods for reference-constrained text-to-image generation.

bird ($\langle o \rangle$) from the reference to synthesize new images with a prompt comprising both these attributes.

We next compare MATTE with P+ and Prospect in Figure 9. First row in each example (one example per column) shows the reference and the attribute from it we seek to

transfer to synthesized images. The phrase under the reference is part of the prompt used to generate new images (e.g., in first column, the prompt is a photo of sunflower following layout $\langle l \rangle$, in the fourth column, the prompt is a $\langle c \rangle$ colored photo of $\langle o \rangle$ in

Metric	$\langle c \rangle$	$\langle o \rangle$	$\langle s \rangle$
Cosine Sim. (CLIP Image-Image)	0.71	0.72	0.92
Cosine Sim. (CLIP Text-Text)	0.74	0.73	0.87

Table 1: CLIP evaluation for tokens learned using MATTE.

Method	layout-color	layout-object	layout-style	color-object	color-style	object-style
P+	0.24	0.22	0.22	0.26	0.20	0.22
ProSpect	0.19	0.24	0.20	0.24	0.19	0.22
MATTE	0.26	0.27	0.24	0.28	0.26	0.26

Table 2: Comparing MATTE with P+ and Prospect.

watercolor style). This is used to generate images with MATTE (shown in the last row in each example). To generate images with P+, we retain the conditioning vectors learned during its inversion process for the layers responsible for the attribute of interest (e.g., in the first column for layout, we retain the set of four coarse prompts a photo of sunflower in $\langle x_i \rangle, i = 1, \dots, 4$, where $\langle x_i \rangle$ is the P+ inverted vector). Similarly, to generate images with Prospect, we retain the vectors learned during its inversion process for timesteps responsible for the corresponding attribute (e.g., for the same layout example, we retain the first three timestep stages prompts).

In the first column in Figure 9, one can note that MATTE (last row) is able to respect both the layout from the reference (four items stacked in a two-by-two fashion) as well as the object of interest (sunflower). On the other hand, in P+ (second-last row), since object and layout are captured in the same coarse layers, it is unable to disentangle them and hence we see an unrelated object (rose) even though the layout is respected from the reference image. Similarly, in Prospect, even though the layout from the reference is respected, it produces red-colored sunflowers. This is because the reference is red in color and Prospect is unable to disentangle color from layout since they are both captured in the same timesteps. Similar observations can be made from the other examples. For instance, in the last column, MATTE (last row) is able to successfully transfer both the learned color and the learned object in generating new cat images in watercolor style. In Prospect, layout, color, and style are all captured in the same timesteps. Consequently, as we retain the conditioning vectors learned for color in this example (it is one of the two attributes we wish to transfer), they happen to be entangled with layout and style, resulting in more images that look exactly like the reference image. In P+, we see cat images that follow the reference’s color but not in the desired watercolor style because color and style are captured in the same layers, making it impossible to disentangle

Metric	$\langle c \rangle$	$\langle o \rangle$	$\langle s \rangle$
$\mathcal{L}_{\mathcal{R}}$	0.62	0.65	0.90
$\mathcal{L}_{\mathcal{R}} + \mathcal{L}_{CS} + \mathcal{L}_{\mathcal{O}}$	0.71	0.72	0.92

Table 3: Ablation results for image-image similarities.

them. These results provide evidence for our key takeaway message- the four attributes can only be disentangled when optimized **jointly** across the timestep and layer dimensions with our proposed loss function in Equation 4. We show additional results, discussion, and limitations in supp.

Quantitative Evaluation. We next quantify the accuracy of the embeddings learned for $\langle c \rangle$, $\langle o \rangle$, and $\langle s \rangle$ from Equation 4 using images from the dataset in (Gal et al. 2022). Note that we are unable to do this for $\langle l \rangle$ due to the absence of a meaningful ground truth label for layouts. For color, we use Color Thief (Dhakar 2015) to extract the ground truth. For object and style, we perform a nearest neighbor lookup using the image’s CLIP embedding (see supplementary for more details). For each reference image, we synthesize 64 new images (using a $\langle c \rangle$ colored photo, a $\langle s \rangle$ style photo, and a photo of $\langle o \rangle$ with various seeds). We also synthesize a set of corresponding 64 ground-truth images using actual ground-truth labels instead of $\langle c \rangle$, $\langle s \rangle$, and $\langle o \rangle$. Given these two sets, we first compute a CLIP-image-based cosine similarity between the synthesized and ground-truth image. We also compute a CLIP-text-based cosine similarity between the prompts for synthesis (that have $\langle c \rangle$, $\langle s \rangle$, and $\langle o \rangle$ tokens) and the ground-truth prompts (that have ground-truth text labels) (results in Table 1). High cosine similarities are indicative of semantic correctness of the learned embeddings for $\langle c \rangle$, $\langle s \rangle$, and $\langle o \rangle$ with our method. We next quantify the improvements with MATTE over P+ and Prospect in Table 2. For every attribute pair, we evaluate how well methods disentangle them. To do this, in each pair, we keep one of them fixed (e.g., layout) from what is learned during inversion (with all three methods) and vary the other (we have a list of 7 style types, 13 object types, and 11 color types following P+, see supp. for details). In each case, we generate the image and compute the CLIP image-text similarity. A higher score indicates better disentanglement since both attributes would then be separately captured well in the output. As can be seen from Table 2, this is indeed the case with MATTE outperforming both P+ and Prospect. Finally, we also conduct an ablation study in Table 3 where the additional losses \mathcal{L}_{CS} and $\mathcal{L}_{\mathcal{O}}$ improve disentanglement by giving higher cosine similarities when compared to $\mathcal{L}_{\mathcal{R}}$.

5 Summary

We presented MATTE, a new algorithm to learn color, object, style, and layout attributes from a reference image and use them for attribute-guided text-to-image synthesis. We first showed existing methods that invert along either the DDPM layer or denoising timestep dimensions are unable to disentangle all the attributes. We then showed that this can be achieved by conditioning both the layer and the timestep dimension as part of the inversion process, leading to our new inversion algorithm that also comprises explicit disentanglement enhancing regularizers. Extensive evaluations show our method is able to accurately extract attributes from reference image and transfer both individual attributes as well as compositions to new generations.

Appendix A

In Section A.1, we show additional results for joint layer-timestep analysis to show further evidence for how certain attributes can be disentangled when both layer and timestep dimension are considered jointly, which otherwise can not be disentangled across a single dimension (as in P+ (Voynov et al. 2023) and ProSpect (Zhang et al. 2023)). In Section A.2, we show more qualitative results for comparing MATTE with baselines. Here we also explain in detail how the prompt conditionings for the baselines P+ and ProSpect are computed. In Section A.3, we talk about the implementation details and the images used for evaluation. In Section A.4, we provide more details on the quantitative evaluation setup followed for reporting the results comparing MATTE with baselines in Table 2 in the main paper. In Section A.5, we report results for a user survey conducted to further compare MATTE with baselines. Finally, we conclude with some discussion on limitations of our method in Section A.6.

A.1 Additional Layer-timestep Analysis

As discussed in the main paper, attributes like `color` and `layout` that are captured along the same timesteps (from Prospect (Zhang et al. 2023)) can be disentangled along the layer dimension. Similarly, geometric attributes like `object` and `layout` that are captured along the same layers (from P+ (Voynov et al. 2023)) can be disentangled along the timestep dimension. We show additional qualitative results to demonstrate the conclusions stated above.

Consider Figure 10 for an example on layout-color disentanglement using joint layer-timestep prompt conditionings. In Figure 10(a), (b) and (c), one can note that we get a `blue ball` despite the color being specified as `red` in the `coarse` layers. In Figure 10(a) and (b), we get a ball placed on a table and under a table respectively as expected, because the corresponding layout conditionings were given as input to all U-Net (Ronneberger, Fischer, and Brox 2015) layers. In Figure 10(c), we notice that we get a ball on a table despite specifying `under a table` in the `moderate` layers. This clearly indicates that the `coarse` layers are dominantly responsible for determining the layout. To summarise, this example shows that while `color` and `layout` are captured along the same timesteps, they can be disentangled along the layer dimension ($L_3 - L_5$ & $L_{10} - L_{13}$ for `color` and $L_6 - L_9$ for `layout`).

Similarly, consider the example in Figure 11, where we show `object` and `layout` that are captured along the same layers can be disentangled along the timestep dimension. Here, based on the final generated image (a standing cow), one can note that the text conditions corresponding to the object `cow` were specified in stage t_2, t_3 and had the most impact on the final image. For instance, despite the input `cat` in t_1 stage, the final image has a cow. Similarly, despite specifying the layout `sitting` in stages t_2, t_3 , the final generation only respected `standing` that was provided in stage t_1 . This shows that while `object` and `layout` are captured along the same layers, they can be disentangled along the timestep dimension (t_2, t_3 for `object` and t_1 for `layout`).

Before we move on to the next example, we had summarised from our analysis in the main paper that fine layers ($L_1 - L_2$ & $L_{14} - L_{16}$) and the stage t_4 have no impact on any of the four attributes. `Color` and `style` are both captured in the initial denoising stages (t_1, t_2) and across moderate U-Net layers ($L_3 - L_5$ & $L_{10} - L_{13}$). Object semantics are captured along the middle denoising stages (t_2, t_3) and across the coarse U-Net layers ($L_6 - L_9$). Finally, `layout` is captured in the very initial denoising stage (t_1) across coarse layers ($L_6 - L_9$).

On that note, we show another example in Figure 12, similar to the joint multi-prompt conditioning example presented in Figure 5 in the main paper, which demonstrates the properties summarised above. For the final generated image (*a blue ball placed on a table*), one can note that the textual conditionings corresponding to each of key attributes in the prompt (`blue`, `ball`, and `on the table`) were specified only across a subset of layers and only along specific timesteps. These observations are consistent with the analysis we summarised for each of the attributes. For instance, despite specifying `white` in $L_1 - L_2$ & $L_{14} - L_{16}$ layers, and `color red` in ($L_6 - L_9$) layers, we still see a `blue` colored ball based on the color specified in moderate ($L_3 - L_5$ & $L_{10} - L_{13}$) layers. Similarly, the layout is captured in the initial stages and across the coarse set of layers. We also show per-layer attention maps across denoising timesteps in Figure 13 which confirms that layout is predominantly captured in layers L_6, L_8 , and L_9 .

A.2 Additional Qualitative Results and Setup Details

We show additional results comparing MATTE with the closest baselines ProSpect (Zhang et al. 2023) and P+ (Voynov et al. 2023). We first explain how we generate images using P+ and ProSpect given a prompt with an example. Consider the example shown in column 1 in Figure 14. The goal here is to generate images of a dog in `oil painting` style following the `color` properties of the reference image. The first step here is to run the inversion algorithms of P+ and ProSpect for the reference image, and get a set of textual conditionings $\langle x_i \rangle$ where $i = 1, \dots, 16$ for P+, and $\langle y_j \rangle$ where $j = 1, \dots, 10$ for ProSpect. Next, depending upon the attributes we want to transfer from the reference image (`color` here), we retain the textual conditionings learned during inversion in P+ and ProSpect as part of the final conditionings used as input along the 16 layers and 10 timestep stages respectively. The decision of retaining conditionings is made on the basis of which set of timesteps/layers are important for capturing the attribute of interest (`color` here). Since we know `color` is captured across the shallow U-Net layers in P+, and across the initial denoising stages in ProSpect, the prompt that goes as input to P+ across the 16 U-Net layers is:

```
[ $\langle x_1 \rangle$  dog in oil painting style,  
 $\langle x_2 \rangle$  dog in oil painting style,  
 $\langle x_3 \rangle$  dog in oil painting style,  
 $\langle x_4 \rangle$  dog in oil painting style,  
 $\langle x_5 \rangle$  dog in oil painting style,  
dog,
```

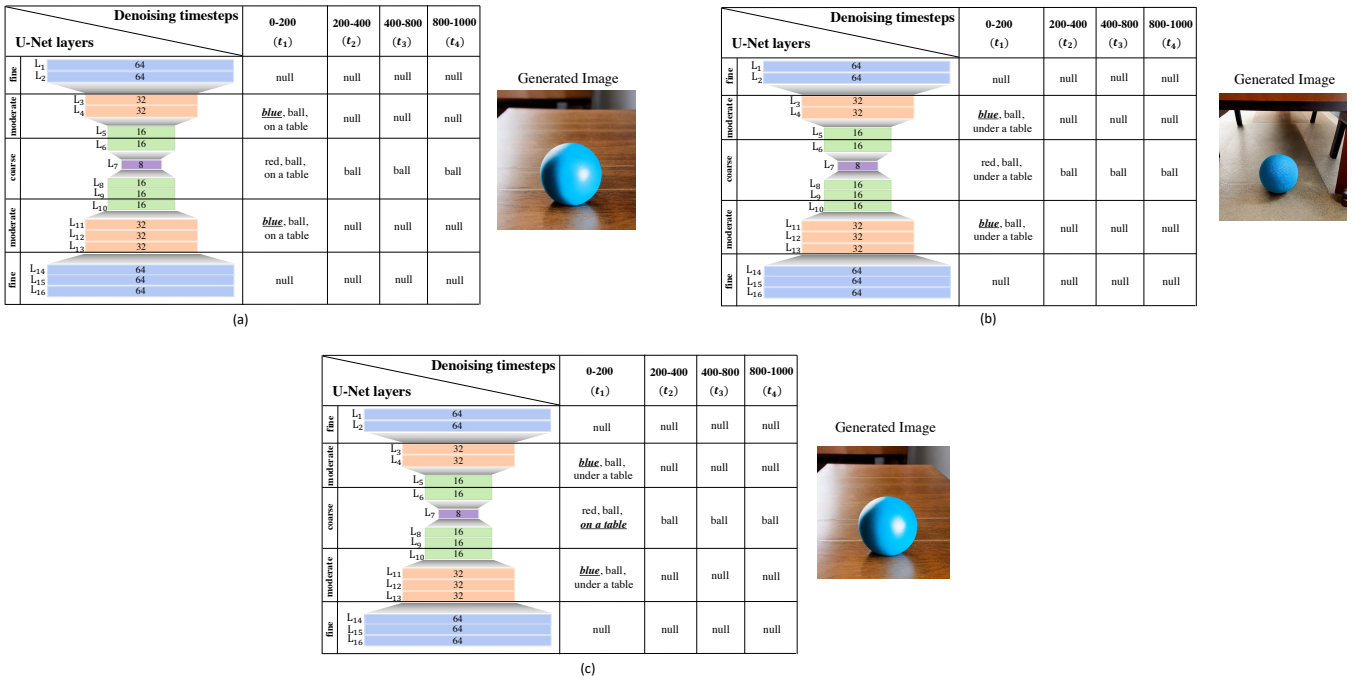


Figure 10: Layout-Color disentanglement.

dog,
dog,
dog,
 $\langle x_{10} \rangle$ dog in oil painting style,
 $\langle x_{11} \rangle$ dog in oil painting style,
 $\langle x_{12} \rangle$ dog in oil painting style,
 $\langle x_{13} \rangle$ dog in oil painting style,
 $\langle x_{14} \rangle$ dog in oil painting style,
 $\langle x_{15} \rangle$ dog in oil painting style,
 $\langle x_{16} \rangle$ dog in oil painting style].

Similarly, the prompt for ProSpect across the 10 denoising timestep stages is:

[$\langle y_1 \rangle$ dog in oil painting style,
 $\langle y_2 \rangle$ dog in oil painting style,
 $\langle y_3 \rangle$ dog in oil painting style,
 $\langle y_4 \rangle$ dog in oil painting style,
dog in oil painting style].

We next discuss the results comparing MATTE with P+ and ProSpect in Figure 14. Consider the example in column 1. Here the goal is to generate a dog in oil painting style while retaining only the color properties from the reference image. We see that MATTE captures everything (dog, oil painting style and color attribute from reference image) accurately. While in ProSpect, even though the colors got transferred from the reference image, but it has gen-

erated dogs following the layout of the inkpot shown in the reference image. This is because, as seen previously, layout and color are captured across similar denoising timesteps, hence disentangling the two is not possible in ProSpect (as inversion in ProSpect is across timestep dimension only). Similarly, for P+, we see that the generated dogs follow the oil painting style but are unable to capture the color of the inkpot. This again is because color and style are captured in same layers in P+, so either color and style both get transferred together or none gets transferred. One can make similar observations across the examples shown in other columns too which clearly indicated that MATTE is able to constrain the generation of images on attributes from reference image in a disentangled fashion much better than the closest baselines.

A.3 Implementation Details and Dataset

We follow the same set of styles, objects and colors as described in P+ (Voynov et al. 2023) for all our evaluations and trainings.

Specifically, during MATTE inversion technique (Section 3.2 in the main paper), the set of styles used to randomly choose styles from was:

["oil painting", "vector art", "pop art style", "3D rendering", "impressionism picture", "graffiti", "fuzzy", "shiny", "bright", "fluffy", "sparkly", "dull", "smooth", "rough", "jagged", "striped", "painting", "retro", "vintage", "modern", "bohemian", "industrial", "rustic", "classic", "contemporary", "futuristic"]

U-Net layers		Denoising timesteps			
		0-200 (t_1)	200-400 (t_2)	400-800 (t_3)	800-1000 (t_4)
fine	L ₁ 64	null	null	null	null
	L ₂ 64				
moderate	L ₃ 32				
	L ₄ 32				
coarse	L ₅ 16				
	L ₆ 16				
	L ₇ 8				
	L ₈ 16				
moderate	L ₉ 16				
	L ₁₀ 16				
	L ₁₁ 32				
moderate	L ₁₂ 32				
	L ₁₃ 32				
	L ₁₄ 64				
fine	L ₁₅ 64				
	L ₁₆ 64				



Figure 11: Layout-Object disentanglement.

For the quantitative evaluations in Section 4 in the main paper, we use the following sets of objects, style and colors (again from P+ (Voynov et al. 2023)):

Objects = ["chair", "dog", "book", "elephant", "guitar", "pillow", "rabbit", "umbrella", "yacht", "house", "cube", "sphere", "car"]

Colors = ["black", "blue", "brown", "gray", "green", "orange", "pink", "purple", "red", "white", "yellow"]

Styles = ["watercolor", "oil painting", "vector art", "pop art style", "3D rendering", "impressionism picture", "graffiti"]

Finally, we show the images used for different evaluation setups in Figure 15.

A.4 Quantitative Evaluation Setup Details

We presented an evaluation to quantify the disentanglement of different pairs of attributes in the main paper in Table 2, Section 4. Here, we explain the details of how we compute the CLIP Image-text similarities reported in the paper. We use the set of images shown in Figure 15 and the set of attributes discussed in Section A.3. For each reference image, our goal was to evaluate the inversion techniques in aspects of (i) preserving/transferring an attribute from the reference image and (ii) generating images following attributes mentioned in the text prompt. We considered 6 unique pairs of attributes for this comparison namely layout-color, layout-object, layout-style, color-object, color-style

and object-style. Consider the case of color-object disentanglement evaluation in the context of reference image based attribute-aware text-to-image generation. The attribute mentioned first (color here) is the one to be transferred from the reference image, whereas the latter (object here) comes from the text prompt. For each of the baselines P+ and ProSpect, we generate final prompt conditionings in the same fashion as explained in Section A.2 by retaining the textual conditionings responsible for capturing the attribute to be transferred from reference image (color here). For the attribute that comes from the text prompt (objects here), we iterate over a set of different objects following the list of objects mentioned in Section A.3 and generate a set of 64 images for each color-object pair. We then compute CLIP Image-text similarities between the generated images and the ground truth object used to generate those images. Similarly, we also compute CLIP Image-text similarities between the generated images and the corresponding ground truth for the attribute to be transferred from reference image wherever possible, followed by an averaging of the two similarities (for color in color-object case, ground truth colors are extracted from the reference image using Color Thief (Dhakar 2015)). Similarly, these CLIP based Image-text similarities are computed for other attribute pairs for MATTE and the closest baselines P+ and ProSpect, results of which are reported in Table 2 in the main paper.

A.5 User Study

We conduct a user study with the generated images where we ask survey respondents to select which set of images (among sets from three different methods, see Table 4) best represents the input constraints. The user is presented with a reference image, a text prompt, and a set of attributes from the reference image that should ideally get transferred to the

U-Net layers		Denoising timesteps			
		0-200 (t_1)	200-400 (t_2)	400-800 (t_3)	800-1000 (t_4)
fine	L ₁	white, lizard, under a table	white, lizard, under a table	white, lizard, under a table	null
	L ₂				
moderate	L ₃	<u>blue</u> , cat, under a table	<u>blue</u> , cat, under a table	green, cat, under a table	null
	L ₄				
coarse	L ₅	red, cat, <u>on a table</u>	red, <u>ball</u> , under a table	red, <u>ball</u> , under a table	null
	L ₆				
moderate	L ₇	<u>blue</u> , cat, under a table	<u>blue</u> , cat, under a table	green, cat, under a table	null
	L ₈				
fine	L ₉	white, lizard, under a table	white, lizard, under a table	white, lizard, under a table	null
	L ₁₀				
moderate	L ₁₁	white, lizard, under a table	white, lizard, under a table	white, lizard, under a table	null
	L ₁₂				
fine	L ₁₃	white, lizard, under a table	white, lizard, under a table	white, lizard, under a table	null
	L ₁₄				
moderate	L ₁₅	white, lizard, under a table	white, lizard, under a table	white, lizard, under a table	null
	L ₁₆				

Generated Image



Figure 12: Multi-prompt conditioning across U-Net layers and denoising timesteps jointly.

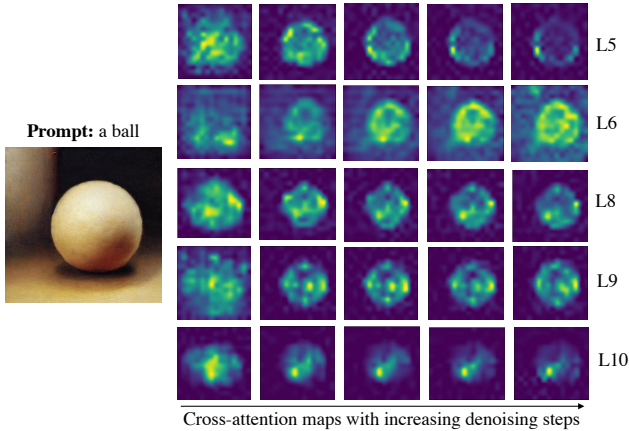


Figure 13: Cross-attention maps for analysing layout.

final generated image (see Figure 16 for an example). From Table 4, our method’s results are preferred by a majority of the survey respondents, thus providing additional evidence for the impact of our proposed inversion technique in constraining text-to-image generation on different attributes of reference images in a disentangled fashion.

A.6 Limitations

In this Section, we briefly discuss a few limitations of MATTE when seen in a constrained text-to-image generation setup. Firstly, the optimization of the embeddings learned for the four tokens namely $\langle c \rangle$, $\langle l \rangle$, $\langle o \rangle$ and $\langle s \rangle$ during inversion is a slow process (MATTE converges faster than TI (Gal et al. 2022), but is

Method	Percentage
P+ (Voynov et al. 2023)	12.2%
ProSpect (Zhang et al. 2023)	13.2%
MATTE	74.6%

Table 4: Results from a user survey with 24 respondents.

still slow), thereby posing a limitation to its’ practical applicability. Secondly, since MATTE doesn’t involve fine-tuning model weights, the final constrained text-to-image generation pipeline after MATTE inverts the reference image into disentangled tokens is limited by the generation abilities of the base diffusion model. For instance, omission of objects mentioned in the text prompt is a known limitation of diffusion models (Agarwal et al. 2023; Chefer et al. 2023; Feng et al. 2022; Liu et al. 2022). So, given a prompt "a $\langle c \rangle$ colored cat playing with a dog" (where $\langle c \rangle$ is extracted from a reference image using MATTE) to the base diffusion model, MATTE will ensure that the cat generated is $\langle c \rangle$ colored but MATTE can not enforce the presence of a cat in the final generated image.

References

- Abdal, R.; Qin, Y.; and Wonka, P. 2019. Image2stylegan: How to embed images into the stylegan latent space? In *Proceedings of the IEEE/CVF international conference on computer vision*, 4432–4441.
- Abdal, R.; Qin, Y.; and Wonka, P. 2020. Image2stylegan++: How to edit the embedded images? In *Proceedings of*

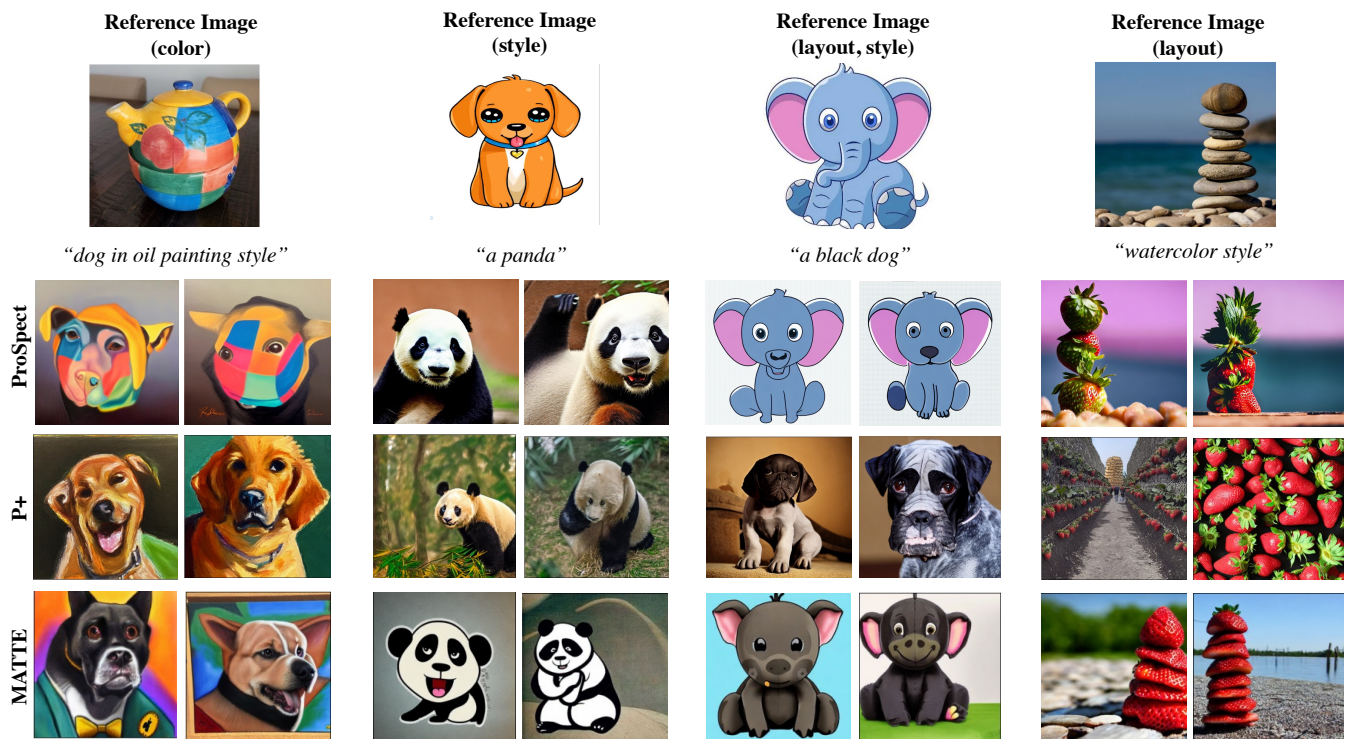


Figure 14: Comparison of MATTE with recent state-of-the-art methods for reference-constrained text-to-image generation.

the IEEE/CVF conference on computer vision and pattern recognition, 8296–8305.

Agarwal, A.; Karanam, S.; Joseph, K.; Saxena, A.; Goswami, K.; and Srinivasan, B. V. 2023. A-STAR: Test-time Attention Segregation and Retention for Text-to-image Synthesis. *arXiv preprint arXiv:2306.14544*.

Alaluf, Y.; Tov, O.; Mokady, R.; Gal, R.; and Bermano, A. 2022. Hyperstyle: Stylegan inversion with hypernetworks for real image editing. In *Proceedings of the IEEE/CVF conference on computer vision and pattern recognition*, 18511–18521.

Bermano, A. H.; Gal, R.; Alaluf, Y.; Mokady, R.; Nitzan, Y.; Tov, O.; Patashnik, O.; and Cohen-Or, D. 2022. State-of-the-Art in the Architecture, Methods and Applications of StyleGAN. In *Computer Graphics Forum*, volume 41, 591–611. Wiley Online Library.

Chefer, H.; Alaluf, Y.; Vinker, Y.; Wolf, L.; and Cohen-Or, D. 2023. Attend-and-Excite: Attention-Based Semantic Guidance for Text-to-Image Diffusion Models. *arXiv preprint arXiv:2301.13826*.

Creswell, A.; and Bharath, A. A. 2018. Inverting the generator of a generative adversarial network. *IEEE transactions on neural networks and learning systems*, 30(7): 1967–1974.

Dhakar, L. 2015. Color thief. Retrieved.

Feng, W.; He, X.; Fu, T.-J.; Jampani, V.; Akula, A.; Narayana, P.; Basu, S.; Wang, X. E.; and Wang, W. Y. 2022. Training-free structured diffusion guidance for compositional text-to-image synthesis. *arXiv preprint arXiv:2212.05032*.

Gal, R.; Alaluf, Y.; Atzmon, Y.; Patashnik, O.; Bermano, A. H.; Chechik, G.; and Cohen-Or, D. 2022. An image is worth one word: Personalizing text-to-image generation using textual inversion. *arXiv preprint arXiv:2208.01618*.

Ho, J.; Jain, A.; and Abbeel, P. 2020. Denoising diffusion probabilistic models. *Advances in neural information processing systems*, 33: 6840–6851.

Kumari, N.; Zhang, B.; Zhang, R.; Shechtman, E.; and Zhu, J.-Y. 2023. Multi-concept customization of text-to-image diffusion. In *Proceedings of the IEEE/CVF Conference on Computer Vision and Pattern Recognition*, 1931–1941.

Lipton, Z. C.; and Tripathi, S. 2017. Precise recovery of latent vectors from generative adversarial networks. *arXiv preprint arXiv:1702.04782*.

Liu, N.; Li, S.; Du, Y.; Torralba, A.; and Tenenbaum, J. B. 2022. Compositional visual generation with composable diffusion models. In *Computer Vision–ECCV 2022: 17th European Conference, Tel Aviv, Israel, October 23–27, 2022, Proceedings, Part XVII*, 423–439. Springer.

Mou, C.; Wang, X.; Xie, L.; Zhang, J.; Qi, Z.; Shan, Y.; and Qie, X. 2023. T2i-adapter: Learning adapters to dig out more controllable ability for text-to-image diffusion models. *arXiv preprint arXiv:2302.08453*.

Nichol, A.; Dhariwal, P.; Ramesh, A.; Shyam, P.; Mishkin, P.; McGrew, B.; Sutskever, I.; and Chen, M. 2021. Glide: Towards photorealistic image generation and editing with text-guided diffusion models. *arXiv preprint arXiv:2112.10741*.

Nitzan, Y.; Aberman, K.; He, Q.; Liba, O.; Yarom, M.; Gandelman, Y.; Mosseri, I.; Pritch, Y.; and Cohen-Or, D. 2022.

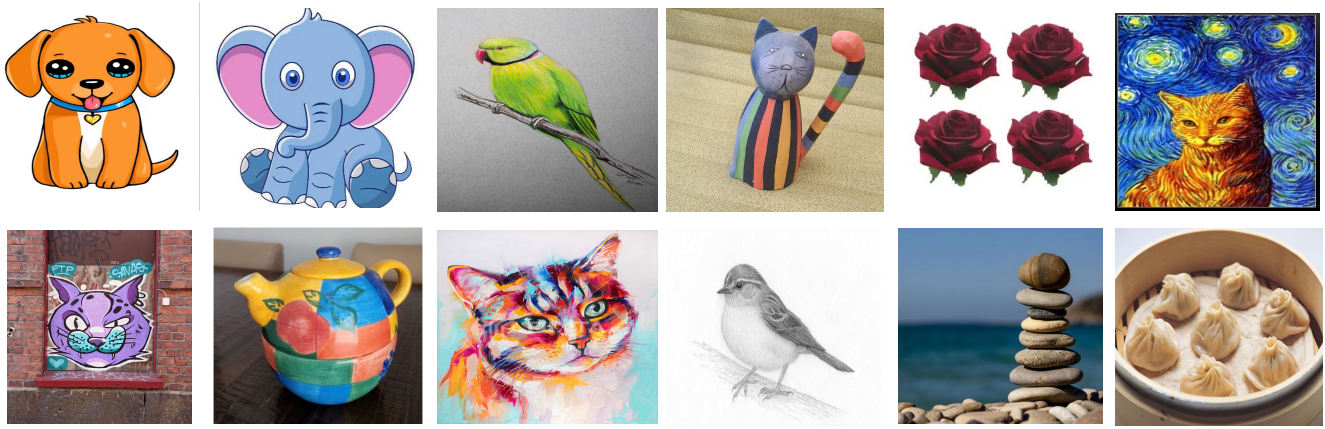


Figure 15: Images used for evaluation.

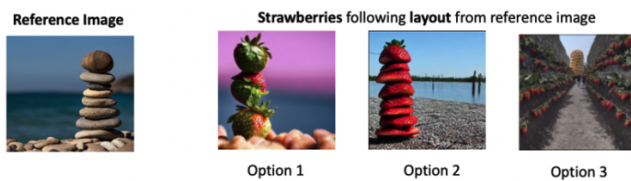


Figure 16: A sample question from the conducted user study.

Mystyle: A personalized generative prior. *ACM Transactions on Graphics (TOG)*, 41(6): 1–10.

Radford, A.; Kim, J. W.; Hallacy, C.; Ramesh, A.; Goh, G.; Agarwal, S.; Sastry, G.; Askell, A.; Mishkin, P.; Clark, J.; et al. 2021. Learning transferable visual models from natural language supervision. In *International conference on machine learning*, 8748–8763. PMLR.

Ramesh, A.; Dhariwal, P.; Nichol, A.; Chu, C.; and Chen, M. 2022. Hierarchical text-conditional image generation with clip latents. *arXiv preprint arXiv:2204.06125*.

Roich, D.; Mokady, R.; Bermano, A. H.; and Cohen-Or, D. 2022. Pivotal tuning for latent-based editing of real images. *ACM Transactions on graphics (TOG)*, 42(1): 1–13.

Rombach, R.; Blattmann, A.; Lorenz, D.; Esser, P.; and Ommer, B. 2022. High-resolution image synthesis with latent diffusion models. In *Proceedings of the IEEE/CVF Conference on Computer Vision and Pattern Recognition*, 10684–10695.

Ronneberger, O.; Fischer, P.; and Brox, T. 2015. U-net: Convolutional networks for biomedical image segmentation. In *Medical Image Computing and Computer-Assisted Intervention—MICCAI 2015: 18th International Conference, Munich, Germany, October 5–9, 2015, Proceedings, Part III 18*, 234–241. Springer.

Ruiz, N.; Li, Y.; Jampani, V.; Pritch, Y.; Rubinstein, M.; and Aberman, K. 2023. Dreambooth: Fine tuning text-to-image diffusion models for subject-driven generation. In *Proceedings of the IEEE/CVF Conference on Computer Vision and Pattern Recognition*, 22500–22510.

Saharia, C.; Chan, W.; Saxena, S.; Li, L.; Whang, J.; Denton, E.; Ghasemipour, S. K. S.; Ayan, B. K.; Mahdavi, S. S.; Lopes, R. G.; et al. 2022. Photorealistic text-to-image diffusion models with deep language understanding. *arXiv preprint arXiv:2205.11487*.

Sohl-Dickstein, J.; Weiss, E.; Maheswaranathan, N.; and Ganguli, S. 2015. Deep unsupervised learning using nonequilibrium thermodynamics. In *International conference on machine learning*, 2256–2265. PMLR.

Song, J.; Meng, C.; and Ermon, S. 2020. Denoising diffusion implicit models. *arXiv preprint arXiv:2010.02502*.

Tewel, Y.; Gal, R.; Chechik, G.; and Atzmon, Y. 2023. Key-locked rank one editing for text-to-image personalization. In *ACM SIGGRAPH 2023 Conference Proceedings*, 1–11.

Voynov, A.; Chu, Q.; Cohen-Or, D.; and Aberman, K. 2023. P+: Extended Textual Conditioning in Text-to-Image Generation. *arXiv preprint arXiv:2303.09522*.

Xia, W.; Zhang, Y.; Yang, Y.; Xue, J.-H.; Zhou, B.; and Yang, M.-H. 2022. Gan inversion: A survey. *IEEE Transactions on Pattern Analysis and Machine Intelligence*, 45(3): 3121–3138.

Zhang, L.; and Agrawala, M. 2023. Adding conditional control to text-to-image diffusion models. *arXiv preprint arXiv:2302.05543*.

Zhang, Y.; Dong, W.; Tang, F.; Huang, N.; Huang, H.; Ma, C.; Lee, T.-Y.; Deussen, O.; and Xu, C. 2023. ProSpect: Expanded Conditioning for the Personalization of Attribute-aware Image Generation. *arXiv preprint arXiv:2305.16225*.